cene Palaeoecology and Palaeohydrology, B. E. Berglund, Ed. (Wiley, Toronto, 1986), pp. 407–422.
20. R. B. Alley *et al.*, *Geology* **25**, 483 (1997); J. Chappellaz *et al.*, *Nature* **366**, 443 (1993); P. A. Mayewski *et al.*, *Science* **263**, 1747 (1994).
21. K. A. Hughen, J. T. Overpeck, L. C. Peterson, S. Trumbore, *Nature* **380**, 51 (1996); J. C. Stager and P. A. Mayewski, *Science* **276**, 1834 (1997); U. von Grafenstein, H. Erlenkeuser, J. Muller, J. Jouzel, S. Johnsen, *Clim. Dyn.* **14**, 73 (1998).
22. G. Bond *et al.*, *Science* **278**, 1257 (1997).
23. Z. C. Yu, J. H. McAndrews, U. Eicher, *Geology* **25**, 251 (1997).

24. We thank J. Denhart, J. N. Haas, S. Hick, R. L. Jefferies, J. H. McAndrews, W. McKenna, L. C. K. Shane, and L. J. Wang for field, laboratory, and general assistance, and L. C. Cwynar, E. Ito, K. Kelts, J. H. McAndrews, D. M. Peteet, L. C. K. Shane, T. Webb III, and H. E. Wright Jr. for discussion and comments. Supported by the Natural Sciences and Engineering Research Council of Canada, Royal Ontario Museum, Ontario Ministry of Education and Training (Ontario Graduate Scholarship), and University of Toronto (Open Fellowships and Department of Botany).

28 April 1998; accepted 13 November 1998

The Percolation Phase Transition in Sea Ice

K. M. Golden,* S. F. Ackley, V. I. Lytle

Sea ice exhibits a marked transition in its fluid transport properties at a critical brine volume fraction p_c of about 5 percent, or temperature T_c of about –5°C for salinity of 5 parts per thousand. For temperatures warmer than T_c, brine carrying heat and nutrients can move through the ice, whereas for colder temperatures the ice is impermeable. This transition plays a key role in the geophysics, biology, and remote sensing of sea ice. Percolation theory can be used to understand this critical behavior of transport in sea ice. The similarity of sea ice microstructure to compressed powders is used to theoretically predict p_c of about 5 percent.

Sea ice is a complex, composite material consisting of pure ice with brine and air inclusions, whose size and geometry depend on the ice crystal structure, as well as the temperature and bulk salinity. It is distinguished from many other porous composites, such as sandstones or bone, in that its microstructure and bulk material properties vary dramatically over a small temperature range. For brine volume fractions p below a critical value $p_c \approx 5\%$, columnar sea ice is effectively impermeable to fluid transport, whereas for p above p_c (>5%), brine or sea water can move through the ice. The relation of brine volume to temperature T and salinity S (*1*) implies p_c corresponds to a critical temperature $T_c \approx -5$°C for $S = 5$ ppt; we refer to this critical behavior as the "law of fives." Perhaps the most direct observations of this are that the time rate of change of sea ice salinity dS/dt due to gravity drainage vanishes for brine volumes below 5% (*2*, *3*) and that the permeability of thin sea ice decreases by more than two orders of magnitude as the surface temperature is lowered, in a small critical region around –5°C (*4*).

Brine transport is fundamental to such processes as sea ice production through freezing of flooded ice surfaces, sea ice heat fluxes, and nutrient replenishment for sea ice algal communities, as well as being an important factor for remote sensing. However, the basic transition controlling brine transport has received little attention. Percolation theory (*5*, *6*) has been developed to analyze the properties of materials where connectedness of a given component determines the bulk behavior. We show that it provides a natural framework to understand the critical behavior of sea ice. In particular, we apply a compressed powder percolation model to sea ice microstructure that explains the law of fives, the observed behavior (*4*) of the fluid permeability in the critical temperature regime, as well as data on surface flooding collected recently on sea ice in the Weddell Sea and East Antarctic regions.

It was observed in the Arctic (*7*) that a snow storm and its resultant loading on a sea ice layer can induce a complete upward flushing of the brine network. In the Antarctic, it was observed that the freezing of a surface slush layer, with resultant brine drainage, induced convection within the ice, whereby rejected dense brine is replaced by nutrient-rich sea water from the upper ocean (*8*), fueling autumn blooms of algae in second-year ice (*9*). During the autumn freeze-up, this process provided about 70% of the salt flux into the upper ocean and increased the total heat flux through the overlying ice and snow cover. The proliferation and growth of sea ice organisms is favored by permeable ice, which allows nutrient replenishment (*10*, *11*). For remote sensing, surface flooding and subsequent freezing can affect microwave backscatter from sea ice (*12*, *13*), and connectedness of the brine inclusions affects the permittivity of sea ice (*14*, *15*). As yet another example, it was observed in the Arctic that there was about a 20-day time lag between the start of the spring snow melt and the occurrence of freshwater input into the mixed layer (*16*, *17*). Presumably, part of this lag was the time it took for the ice sheet to warm to above the critical temperature to allow drainage out of the ice (*16*).

Percolation theory (*5*, *6*) has been used to successfully model a broad array of disordered materials and processes. The simplest form of the lattice percolation model (*6*) is defined as follows. Consider the d-dimensional integer lattice $\mathbf{Z}^d$ and the square (or cubic) network of bonds joining nearest neighbor lattice sites. To each bond, with probability p, $0 \le p \le 1$, we assign a 1, meaning it is open, and with probability $1 - p$ we assign a 0, meaning it is closed. Groups of connected open bonds are called open clusters, and the size of a cluster is just the number of open bonds it contains. In the percolation model, there is a critical probability p_c, $0 < p_c < 1$, called the percolation threshold, at which the average cluster size $\chi(p)$ diverges and an infinite cluster appears, so that the open bonds percolate. In two dimensions, $p_c = 0.5$; in three dimensions, $p_c \approx 0.25$. For $p > p_c$, the infinite cluster density $P_\infty(p)$ exhibits power law behavior near the threshold, $P_\infty(p) \sim (p - p_c)^\beta$, where β is the percolation critical exponent, $\beta \le 1$. This model deals only with the geometrical aspects of connectedness in disordered media, yet we are interested in the transport properties as well. Then we consider a random resistor network, where the bonds are assigned the conductivities 1 and $h \ge 0$ with probabilities p and $1 - p$. With $h = 0$, for $p < p_c$, the effective conductivity $\sigma(p) = 0$, whereas near the threshold with $p > p_c$, $\sigma(p)$ exhibits power law behavior $\sigma(p) \sim (p - p_c)^t$, where t is the conductivity critical exponent, with $1 \le t \le 2$ in $d = 2,3$ (*18*). Analogously, we may consider a random pipe network with effective fluid permeability $\kappa(p)$ exhibiting similar behavior $\kappa(p) \sim (p - p_c)^e$, where e is the permeability critical exponent, with $e = t$. Critical exponents for lattice models are generally believed to exhibit universality, meaning that they depend only on dimension and not on the type of lattice, although continuum models can exhibit nonuniversal behavior, with exponent values different from the lattice case, $t > 2$ in $d = 3$, and $e \neq t$.

If the above lattice model is applied to sea ice, where the open bonds represent brine and the closed bonds represent ice, then p_c would be about 25% in $d = 3$, which is much larger than the observed 5%. Even continuum models, such as ellipsoidal brine inclusions randomly distributed in an ice host (a commonly used model for sea ice), exhibit critical volume fractions in the 20 to 40% range (*19*). Instead,

K. M. Golden, Department of Mathematics, University of Utah, Salt Lake City, UT 84112, USA. S. F. Ackley, U.S. Army Cold Regions Research and Engineering Laboratory, Hanover, NH 03755, USA. V. I. Lytle, Antarctic Cooperative Research Centre and Australian Antarctic Division, University of Tasmania, Hobart, Tasmania 7001, Australia.

*To whom correspondence should be addressed. E-mail: golden@math.utah.edu

consider the critical behavior of composites made up of conducting particles suspended in an insulating matrix (*20*) and the problem of finding microstructures that reduce p_c. For some flexible polymer composites designed to be highly conducting, it was found that by compacting powders of large polymer particles with much smaller metal particles, low critical volume fractions of the (more expensive) metal particles are required to significantly lower the resistance of the composite (*21, 22*). The resulting microstructure of such compressed powders is remarkably similar to the cellular microstructure of columnar sea ice (Fig. 1). The key parameter in predicting the conduction threshold for compressed powders is the ratio $\xi = R_p/R_m$ of the radii of the large polymer particles to the smaller metal particles (*22, 23*). For large ξ, p_c is not very sensitive to the exact value of ξ. For example, a range of 44 to 17 for ξ gives only a range of 3 to 7% for p_c. Using photomicrographs of sea ice microstructure and typical brine inclusion sizes (*3*), we measured the corresponding parameter for sea ice, obtaining an average of $\xi \approx 24$. Applying the compressed powder percolation model (*23*) yields a critical brine volume for columnar sea ice of about 5%. This result will vary with ice crystal structure. For example, the slightly higher values of p_c (lower ξ) observed in (*4*) are caused by the more random distributions of brine inclusions in granular ice as compared to columnar ice. The compressed powder model explains why sea ice exhibits such low values for p_c, as compared to the 20 to 40% range that might be expected, and provides reasonable estimates for p_c, which depends only on the geometry of the two phases. Observations show, however, that fluid transport then proceeds primarily through large-diameter brine channels (*3, 8, 9*). Dynamic models will likely be needed for analysis of brine-channel formation beyond the initial onset of percolation at p_c, although it is interesting to note the existence of the "independent crossings" of a sample in standard percolation models (*24*). They have large separations in comparison to the microstructural (or lattice spacing) scale for p near p_c and play much the same role for transport as the brine channels.

Comparison of the electrical conductivity of compressed powders and the fluid permeability of sea ice (Fig. 2) shows that near the critical temperature, sea ice permeability displays the same characteristic behavior exhibited, in general, by transport coefficients of composite media near a percolation threshold (*19, 20*). The data in (Fig. 2B) are thus best fit not with a straight line as in (*4*) but with an "S" curve that captures the actual behavior of $\kappa(T)$ in the critical regime near the percolation threshold T_c^{perc}.

Compressed powders with low p_c exhibit large, nonuniversal values of t ranging between 2 and 7 (*20*). A rough estimate for the fluid permeability critical exponent e for sea ice based on the data in (Fig. 2B) is about 2.5, although there is significant uncertainty in this estimate (but e is probably between 2 and 4). Much more experimental work needs to be done to determine the actual range of e and its dependence on the type of sea ice and on other factors.

Data collected on Antarctic sea ice directly demonstrate the significance of the percolation threshold. During the winter ANZFLUX experiment (*25*) in the Eastern Weddell Sea, we encountered a thin ice pack, typically 20 to 60 cm thick. Unusually large vertical oceanic heat fluxes resulted in ice basal melt rates of up to 3 cm/day (average was 1 cm/day), which could have melted the ice in a short period. The persistence of the ice depended on flooding of the surface and the subseqent freezing of this slushy snow/brine mixture to form snow ice, which replaced the ice melting on the bottom (*26*). The surface flooding was controlled by upward brine percolation. Temperature profiles measured hourly during a 5-day drift camp over Maud Rise at about 4°E longitude and 65°S latitude (Fig. 3) indicated that while most of the sea ice layer remained above the critical temperature for percolation, the top 5 cm or so of the sea ice was impermeable, except during the typically warm storms. Sufficient loading led to surface flooding, which subsequently froze. This cyclic process occurred twice during the 5-day drift. The impermeable layer, defined by temperatures below a critical temperature of about –5.3°C, disappeared with the onset of the first storm during day 216 of the year (4 August 1994). For about a day, the entire ice sheet was permeable, and by noon of the next day, we observed a thick layer of slushy snow consisting of 30 to 50% liquid brine. Subsequently, a cold

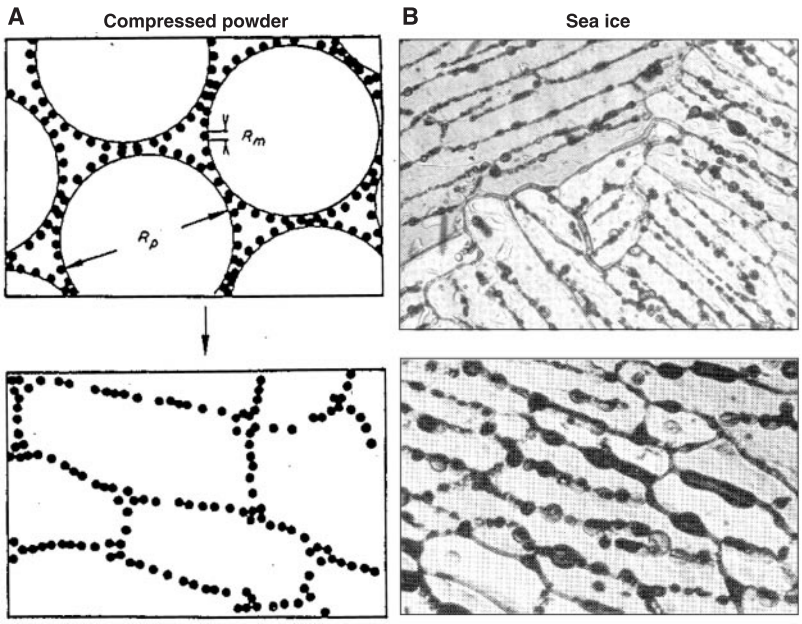

Fig. 1. Comparison of the microstructures of (**A**) compressed powder of large polymer particles of radius R_p and small metal particles of radius R_m (*22*), and (**B**) sea ice (*29*).

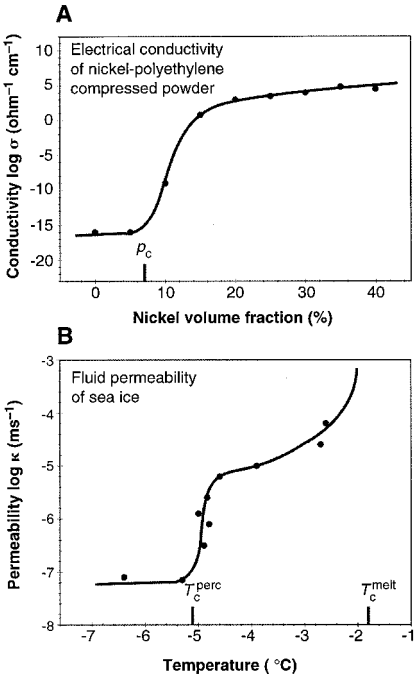

Fig. 2. Comparison of (**A**) the electrical conductivity of compressed powders of large polyethylene particles of radius R_p and small nickel particles of radius R_m, where $\xi = R_p/R_m = 16$ [data points from (*22*)], and (**B**) the fluid permeability $\kappa(T)$ of thin young sea ice as a function of surface temperature [data points from (*4*)]. The transport properties of both materials exhibit critical behavior characteristic of a percolation transition. We have also indicated a second transition for $\kappa(T)$ at the melting point T_c^{melt}, where log $\kappa(T)$ must increase rapidly.

period set in, the slush froze, and the impermeable cap returned as frozen slush. Then another storm moved in, with resultant warming, flooding, and freezing. Late in the evening of day 219 during a warm storm, we observed large "boils" on the snow surface, which was apparently brine percolating up through the ice.

A similar type of flooding event was observed during the winter HIHO HIHO experiment (*27*) in the East Antarctic sea ice pack at about 145°E and 65°S. Brine volumes were calculated using measured salinity and temperature profiles (Fig. 4). The initial brine volume of the ice was near, yet below, the percolation threshold. As air temperatures increased, brine volume throughout the ice sheet was raised above the percolation threshold of $p_c \approx 5\%$ (and in the upper 15 cm was even raised above a higher p_c for granular ice), resulting in surface flooding of the snow, which covered the sea ice. This saturated snow froze, forming snow ice. Ice and snow thickness measured before (day 230, 18 August 1995) and after (day 236) the flooding indicate that 9.5 cm of snow ice had formed. These data demonstrate that an air temperature increase alone can cause the permeability phase transition.

As a final example, consider the algal bloom observed in a porous sea ice layer at a depth of 10 to 30 cm during the autumn of 1992 in the western Weddell Sea (*9*). From day 60 (29 February) to 81 of the year, standing stocks of pigments in the ice increased at a rate of 0.8 mg m^{-1} day^{-1}, yet after day 81, the algal growth rate was reduced to one-tenth the earlier value. Day 81 is when the downward advancing critical isotherm of $T_c \approx -4$°C passed through the bottom of the algal layer, effectively cutting off the community from significant nutrient replenishment, because ice above this isotherm was impermeable. The critical temperature higher than –5°C is understood by noting that the ice surrounding the algal layer was granular, and had a higher p_c, yet a salinity of only about 5 ppt.

It has been demonstrated that sea ice exhibits a percolation transition at a critical temperature. Recently, it has been found that this type of behavior in composite materials is mathematically analogous to a phase transition in statistical mechanics, like water at its freezing point or a ferromagnet at its Curie point (*28*). Thus, T_c may be viewed as a type of phase transition point, with sea ice at temperatures between T_c and –1.8°C (the freezing point for sea water) being a hybrid phase between liquid and solid.

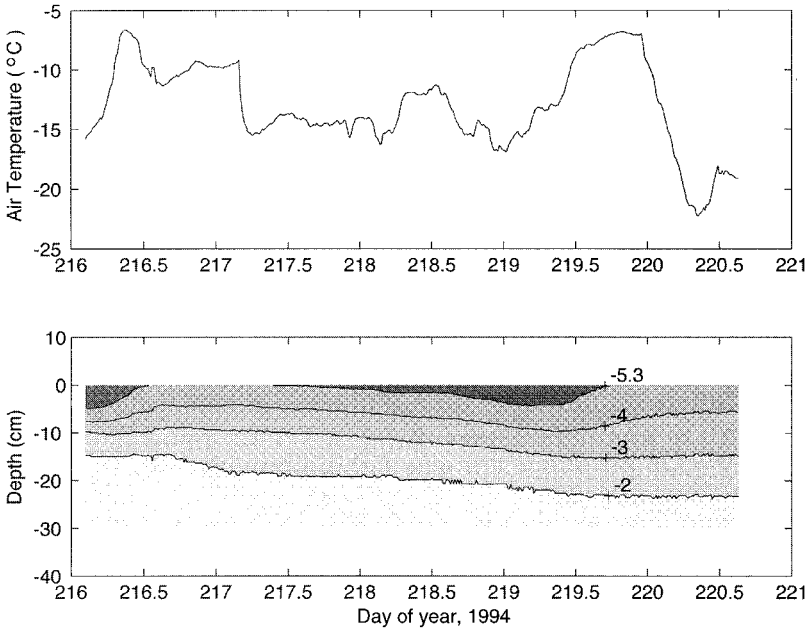

Fig. 3. Temperature contours in sea ice during the Maud Rise drift camp of the ANZFLUX experiment in the Eastern Weddell Sea (bottom), along with air temperatures (top). The black top layer represents ice which is effectively impermeable to fluid transport and is not present during warm storms, so that brine may percolate to the surface. Subsequent freezing of the slush layer is an important ice growth mechanism in the region.

Fig. 4. Brine volume contours in sea ice during the HIHO HIHO experiment in the East Antarctic sea ice zone. An abrupt increase in air temperature late on day 231 resulted in the entire sea ice layer having brine volumes above the percolation threshold of $p_c \approx 5\%$, rendering it permeable to brine transport. Brine then infiltrated the surface, and the resulting slush layer later froze, forming snow ice.

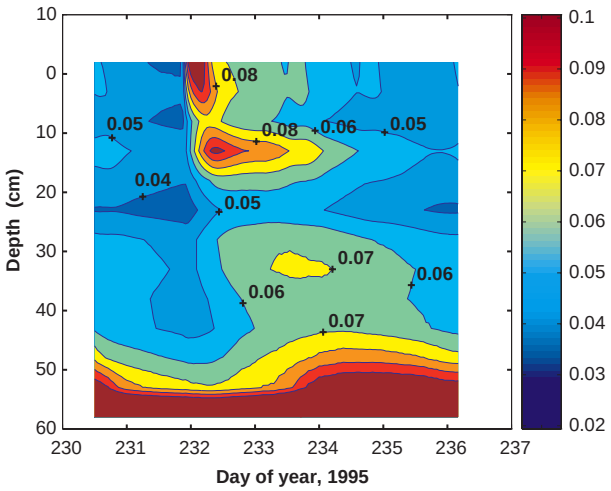

References and Notes

1. G. Frankenstein and R. Garner, *J. Glaciol.* **6**, 943 (1967).
2. G. F. N. Cox and W. F. Weeks, *Brine Drainage and Initial Salt Entrapment in Sodium Chloride Ice*, CRREL Research Report 354 (Cold Regions Research and Engineering Laboratory, Hanover, NH, 1975).
3. W. F. Weeks and S. F. Ackley, *The Growth, Structure and Properties of Sea Ice*, CRREL Monograph 82-1 (Cold Regions Research and Engineering Laboratory, Hanover, NH, 1982).
4. N. Ono and T. Kasai, *Ann. Glaciol.* **6**, 298 (1985).
5. S. R. Broadbent and J. M. Hammersley, *Proc. Cambridge Philos. Soc.* **53**, 629 (1957).
6. D. Stauffer and A. Aharony, *Introduction to Percolation Theory* (Taylor & Francis, London, ed. 2, 1992).
7. E. J.-J. Hudier and R. G. Ingram, *Atmos. Ocean* **33**, 569 (1995).
8. V. I. Lytle and S. F. Ackley, *J. Geophys. Res.* **101**, 8853 (1996).
9. C. H. Fritsen, V. I. Lytle, S. F. Ackley, C. W. Sullivan, *Science* **266**, 782 (1994).
10. G. S. Dieckmann, M. A. Lange, S. F. Ackley, J. C. Jennings, *Polar Biol.* **11**, 449 (1991).
11. H. Eicken, *ibid.* **12**, 3 (1992).
12. A. R. Hosseinmostafa *et al.*, *J. Electromagn. Waves Appl.* **9**, 421 (1995).
13. V. I. Lytle and K. M. Golden, *Antarct. J. U.S.* **30**, 125 (1995).
14. K. M. Golden, in *Wave Propagation in Complex Media, IMA Volumes in Mathematics and its Applications*, vol. 96, G. Papanicolaou, Ed. (Springer-Verlag, Berlin, 1997), pp. 75–94.
15. K. M. Golden *et al.*, *IEEE Trans. Geosci. Remote Sens.* **36**, 1655 (1998).
16. M. G. McPhee, personal communication.
17. G. A. Maykut and M. G. McPhee, *J. Geophys. Res.* **100**, 24691 (1995).
18. K. Golden, *Phys. Rev. Lett.* **65**, 2923 (1990).
19. S. DeBondt, L. Froyen, A. Deruyttere, *J. Mater. Sci.* **27**, 1983 (1992).
20. D. S. Mclachlan, M. Blaszkiewicz, R. E. Newnham, *J. Am. Ceram. Soc.* **73**, 2187 (1990).
21. R. P. Kusy and D. T. Turner, *Nature* **229**, 58 (1971).
22. A. Malliaris and D. T. Turner, *J. Appl. Phys.* **42**, 614 (1971).
23. R. P. Kusy, *ibid.* **48**, 5301 (1977). An approximate formula for the critical volume fraction for percolation of the small metal spheres in a compressed

powder is given by $p_c = [1 + \xi \phi/(4 x_c)]^{-1}$, where ϕ is a reciprocal planar packing factor, and x_c is a critical surface area fraction of the larger particles, which must be covered for percolation by the smaller particles. Values based on microstructural analysis giving good agreement with conductivity experiments are $x_c = 0.42$ and $\phi = 1.27$, which we have also used as a reasonable approximation for sea ice.

24. J. T. Chayes and L. Chayes, *Commun. Math. Phys.* **105**, 133 (1986).
25. M. G. McPhee *et al.*, *Bull. Am. Meteorol. Soc.* **77**, 1221 (1996).
26. S. F. Ackley, V. I. Lytle, K. M. Golden, M. N. Darling, G. A. Kuehn, *Antarctic J. U.S.* **30**, 133 (1995).
27. V. I. Lytle, R. Massom, N. Bindoff, A. P. Worby, I. Allison, *J. Geophys. Res.*, in press.
28. K. M. Golden, *Phys. Rev. Lett.* **78**, 3935 (1997).
29. S. A. Arcone, A. J. Gow, S. McGrew, *J. Geophys. Res.* **91**, 14281 (1986).
30. We thank the participants of the ANZFLUX and HIHO HIHO experiments and the crews of the *R.V. Nathaniel B. Palmer* and the *R.S.V. Aurora Australis* for contributing to the field work yielding the data we report. We also thank M. McPhee, D. Perovich, H. Eicken, and A. Efros for helpful discussions and P. Heil, A. Worby, and two anonymous reviewers for helpful comments on the manuscript. Supported by NSF grants OPP-97-25038, DMS-96-22367, and Office of Naval Research grant N00014-93-10141 to K.M.G. and NSF grant OPP-93-15934 to S.F.A.

16 September 1998; accepted 10 November 1998

Evidence for Extreme Climatic Warmth from Late Cretaceous Arctic Vertebrates

J. A. Tarduno,* D. B. Brinkman, P. R. Renne, R. D. Cottrell, H. Scher, P. Castillo

A Late Cretaceous (92 to 86 million years ago) vertebrate assemblage from the high Canadian Arctic (Axel Heiberg Island) implies that polar climates were warm (mean annual temperature exceeding 14°C) rather than near freezing. The assemblage includes large (2.4 meters long) champsosaurs, which are extinct crocodilelike reptiles. Magmatism at six large igneous provinces at this time suggests that volcanic carbon dioxide emissions helped cause the global warmth.

The Cretaceous is commonly considered to have been ice-free with high atmospheric CO_2 levels (*1*–*3*), but some isotopic and paleofloral evidence has implied that polar temperatures were near freezing (*4*–*6*). Here we describe a fossil vertebrate assemblage from the high Canadian Arctic that supports a Late Cretaceous [92 to 86 million years ago (Ma)] thermal maximum.

The Cretaceous of the Canadian Arctic is represented by sedimentary and volcanic rocks of the Sverdrup Basin (*7*), which are exceptionally well exposed on western Axel Heiberg Island (Fig. 1). The youngest rocks in the area are Late Cretaceous to Eocene sedimentary rocks of the Eureka Sound Group. Shallow marine to continental shale, siltstone, and sandstone are underlain by Late Cretaceous marine shale of the Kanguk Formation. On much of western Axel Heiberg Island, the Kanguk Formation unconformably overlies subaerially erupted flood basalts of the Cretaceous Strand Fiord Formation. These lavas are part of a large magmatic pulse, or large igneous province, that may include large parts of Ellesmere Island and the Arctic Ocean basin (*8*).

Near Expedition Fiord (79°23.5′N, 92° 10.9′W), sedimentary rocks record the transition between the Strand Fiord lavas and Kanguk shale. The uppermost flow of the Strand Fiord Formation is overlain by 0.6 m of weathered basalt and soil (Fig. 1). The soil is overlain by approximately 3.0 m of shale and siltstone, which may represent a bay or estuary. We found well-preserved vertebrate fossils in several of the thin siltstone horizons in this sequence. Although disarticulated, related bones were in close proximity, suggesting limited transport.

Recent magnetostratigraphic study (*9*) at Strand Fiord (Fig. 1) suggests that the base of the Kanguk Formation is older than 83.5 Ma (geomagnetic chron 33R) (*10*). Ammonites of the *Scaphites depressus* Zone indicate that the Kanguk Formation 194 m above its base at Glacier Fiord (*11*) is of late Coniacian age (~86.0 to 87.0 Ma). Ammonites suggest that the basal Kanguk Formation is late early Turonian in age (~92.0 to 91.0 Ma) on Amund Ringes Island (*7*). $^{40}Ar/^{39}Ar$ incremental heating (*12*) of a whole-rock sample from the upper lava flows at Strand Fiord (*9*) has yielded an 11-step plateau (Fig. 2). These data indicate an age of 95.3 ± 0.2 Ma near the Cenomanian-Turonian boundary (*13*). U/Pb zircon analyses of gabbroic intrusions on northwestern Ellesmere Island, thought to be part of the same magmatic event as that represented by the Strand Fiord Formation, yield an age of 92.0 ± 1.0 Ma (early Turonian) (*14*). Together these data indicate that the vertebrate fossil assemblage is Turonian to Coniacian (~92 to 86 Ma) in age.

The fossils represent a diverse assemblage of nonmarine aquatic and semiaquatic vertebrates (Fig. 3), including fish, turtles, and champsosaurs. At least two types of fish are represented by scales similar to those described as Holostean A and Holostean B from Upper Cretaceous nonmarine sediments (*15*). Turtles and champsosaurs offer several advantages over other fossils used as climatic indicators, such as the latest Cretaceous dinosaurs of the North Slope, Alaska, because they are free from ambiguities posed by possible migration and warm-bloodedness (*16*, *17*). Turtles are represented by costals and peripherals that are comparable to shell elements of generalized aquatic cryptodires. Extant aquatic nonmarine turtles are ectothermic reptiles and have a climatically limited distribution. The length and warmth of summers limit turtle distributions, primarily by affecting the survival of eggs and hatchlings. The cold-adapted turtles *Chelydra serpentina* and *Chrysemys picta* provide a conservative estimate of the growing season required (*18*). Viable populations of these taxa are restricted to areas where the growing season has at least 100 frost-free days per year (*19*).

Maximum temperatures during the warmest month of the year also provide a measure of the climatic requirements of these cold-adapted turtles. Naturally occurring viable populations of *Chelydra serpentina* and *Chrysemys picta* do not occur in areas with a warm-month average maximum temperature of less than 25°C (*18*, *19*). This measure corresponds to a warm-month mean temperature of 17.5°C and a mean annual temperature of 2.5°C. Thus, by analogy, the turtles in the Late Cretaceous Axel Heiberg locality indicate that the mean annual temperature was at least 2°C, the warm-month average maximum temperature was at least 25°C, and the climate was frost-free for more than 100 days per year.

The Axel Heiberg vertebrate assemblage differs from others known from the Upper Cretaceous of Arctic North America in the abundance of semiaquatic reptiles (*20*) and in the presence of champsosaurs. Champsosaurs, which are thought to have been active semiaquatic predators (*21*), are represented by a tibia, a mandible, an ulna, femurs, ribs, gastralia, ischia, and centra (Fig. 3). The mandible fragment indicates that the snout was long and

J. A. Tarduno, R. D. Cottrell, H. Scher, Department of Earth and Environmental Sciences, University of Rochester, Rochester, NY, 14627, USA. D. B. Brinkman, Royal Tyrrell Museum of Palaeontology, Drumheller, Alberta, TOJ OYO, Canada. P. R. Renne, Berkeley Geochronology Center, Berkeley, CA 94709, USA. P. Castillo, Geological Research Division, Scripps Institution of Oceanography, La Jolla, CA 92093–0220, USA.

*To whom correspondence should be addressed. E-mail: john@earth.rochester.edu